The EMBO Journal vol.15 no.9 pp.2160–2168, 1996

Characterization of a redox active cross-linked complex between cyanobacterial photosystem I and soluble ferredoxin

Cécile Lelong[1], Egbert J.Boekema[2,3], Jochen Kruip[4], Hervé Bottin[1], Matthias Rögner[4] and Pierre Sétif[1,3]

[1]CEA, Département de Biologie Cellulaire et Moléculaire, C.E. Saclay, 91191 Gif-sur-Yvette Cedex, France, [2]Biofysische Chemie, Rijksuniversiteit Groningen, Nijenborgh 4, 9747 AG Groningen, The Netherlands and [4]Institut für Botanik, Universität Münster, Schlossgarten 3, D-48149 Münster, Germany

[3]Corresponding authors

A covalent stoichiometric complex between photosystem I (PSI) and ferredoxin from the cyanobacterium *Synechocystis* sp. PCC 6803 was generated by chemical cross-linking. The photoreduction of ferredoxin, studied by laser flash absorption spectroscopy between 460 and 600 nm, is a fast process in 60% of the covalent complexes, which exhibit spectral and kinetic properties very similar to those observed with the free partners. Two major phases with $t_{1/2}$ <1 μs and ≈10–14 μs are observed at two different pH values (5.8 and 8.0). The remaining complexes do not undergo fast ferredoxin reduction and 20–25% of the complexes are still able to reduce free ferredoxin or flavodoxin efficiently, thus indicating that ferredoxin is not bound properly in this proportion of covalent complexes. The docking site of ferredoxin on PSI was determined by electron microscopy in combination with image analysis. Ferredoxin binds to the cytoplasmic side of PSI, with its mass center 77 Å distant from the center of the trimer and in close contact with a ridge formed by the subunits PsaC, PsaD and PsaE. This docking site corresponds to a close proximity between the [2Fe–2S] center of ferredoxin and the terminal [4Fe–4S] acceptor F_{II} of PSI and is very similar in position to the docking site of flavodoxin, an alternative electron acceptor of PSI.

Keywords: cyanobacteria/electron microscopy/ferredoxin/photosystem I/spectroscopy

Introduction

The interactions of soluble ferredoxin with its numerous partners are still poorly understood, despite its major role in bioenergetic pathways in oxygen-evolving photosynthetic organisms (Knaff and Hirasawa, 1991). A noticeable exception is the interaction of ferredoxin with ferredoxin-NADP reductase (FNR). These last interactions were studied in depth through the combined use of many different approaches, including enzymologic studies (Batie and Kamin, 1984a,b), chemical modification (Medina *et al.*, 1992; Jelesarov *et al.*, 1993), cross-linking studies (Zanetti *et al.*, 1988), site-directed mutagenesis of both partners (Hurley *et al.*, 1993a,b, 1994; Aliverti *et al.*, 1994) and laser flash kinetic studies of electron transfer (Bhattacharyya *et al.*, 1986; Walker *et al.*, 1991). A structural model of these interactions can also be derived from the structure of phthalate dioxygenase reductase (Correll *et al.*, 1992), which can be considered as a chimeric protein containing both ferredoxin and FNR domains, whereas differing models have been proposed for the ferredoxin–FNR complex (De Pascalis *et al.*, 1993; Karplus and Bruns, 1994). By contrast, little is known regarding the interactions of ferredoxin with its many other soluble partners (see, however, Hirasawa *et al.*, 1987, 1991, 1994a,b; De Pascalis *et al.*, 1994). Our present knowledge of the interactions between ferredoxin and photosystem I (PSI) reaction centers is intermediate between these two extreme situations. Whereas a rather detailed picture of the kinetics of ferredoxin reduction by PSI has emerged recently (Sétif and Bottin, 1994, 1995), the structural characterization of the complex is very poor. A possible model for the PSI–ferredoxin complex has been proposed recently (Fromme *et al.*, 1994), which was based on the X-ray structures of PSI from the cyanobacterium *Synechococcus elongatus* determined at 6 Å resolution (Krauss *et al.*, 1993) and of ferredoxin from the cyanobacterium *Spirulina platensis* (Tsukihara *et al.*, 1981).

The X-ray PSI structure allowed the precise localization of the iron–sulfur centers of PSI within its global structure, as these centers correspond to high electron densities (Krauss *et al.*, 1993). PSI contains three [4Fe–4S] centers, named F_A, F_B and F_X, which are the terminal electron acceptors (for a review, see Golbeck, 1993). F_X is known to be associated with the two large membrane subunits of PSI named PsaA and PsaB, constituting a bridge between these two subunits. Centers F_A and F_B exhibit different electon paramagnetic resonance (EPR) properties and redox potentials and are associated with the small peripheral subunit PsaC which is analogous to some bacterial ferredoxins. Electron density associated with F_X could be assigned unambiguously, but discrimination between F_A and F_B is still not possible: whereas one of these (named F_I) is clearly located closer to the membrane plane than the other one (named F_{II}), the identification of F_I with F_A or F_B (and conversely of F_{II} with F_B or F_A) is still unclear. It is also most likely that soluble ferredoxin is reduced by $(F_I, F_{II})^- [(F_A, F_B)^-]$ (Sétif and Bottin, 1994), though it is not yet known whether the direct partner of ferredoxin is F_I^- or F_{II}^-.

Analysis of electron micrographs of PSI isolated from wild-type and mutants with specifically deleted subunits yielded a model for the localization of these subunits within PSI (Kruip *et al.*, 1995). Particularly, it was shown by electron microscopy that the PsaC, PsaD and PsaE subunits of PSI nearly exclusively make up that part of the PSI complex which protrudes into the cytoplasm

(Kruip *et al.*, 1993). On the other hand, it has been shown that both PsaD and PsaE subunits play a major role in the interactions of PSI with ferredoxin (Zanetti and Merati, 1987; Zilber and Malkin, 1988; Andersen *et al.*, 1992; Rousseau *et al.*, 1993; Sonoike *et al.*, 1993; Lelong *et al.*, 1994). Despite these studies, it is rather obvious that a structural model of the PSI–ferredoxin complex is still lacking. In the present report, the approximate location of ferredoxin within a chemically cross-linked complex with PSI is reported and compared with that of flavodoxin. A detailed functional characterization of this complex is also made by flash absorption spectroscopy. These structure–function relationships allow the further characterization of the possible electron transfer pathways which are compatible with the kinetic observations of ferredoxin reduction by PSI. A comparison with the covalent complex between PSI and flavodoxin can also be made, showing that both proteins share a common binding region on the PSI reaction center.

Results

Flash absorption spectroscopy of ferredoxin reduction

Transient signals were recorded by laser flash absorption spectroscopy of a PSI preparation to which ferredoxin has been cross-linked and of a control sample pre-treated with the chemical cross-linker in the absence of ferredoxin. This is shown in the upper part of Figure 1 where the decay of $P700^+$ (P700 being the primary electron donor of PSI) has been monitored at pH 8.0 for the control (left curve) and the cross-linked sample (right curve) on a long time scale of ~5 s. In the control sample, the decay of $P700^+$ is bi-exponential [see residuals (2) below the curve]. This behavior is thought to result from a competition process between (i) charge recombination between $P700^+$ and the reduced terminal acceptor $(F_A, F_B)^-$ (rate: k_r) and (ii) electron escape from $(F_A, F_B)^-$ to exogenous acceptors (rate: k_e). The faster rate of the biphasic decay corresponds to the rate ($k_r + k_e$) ($\approx$15.1 s^{-1}) whereas the slow decay (rate k_d $\approx$0.112 s^{-1}) corresponds to the subsequent slow reduction of $P700^+$ by the exogenous electron donor, reduced 2,6-dichlorophenol-indophenol (DPIP), in those reaction centers where electron escape has occurred. By contrast to the control sample, the decay of $P700^+$ in the cross-linked sample cannot be fitted satisfactorily by only two exponential components [residuals (2)] but can be described by three different components [residuals (3)]. The fastest and slowest rates resulting from this three-exponential fit are very similar to those found in the control sample. The third component exhibits a rate of 0.84 s^{-1} ($t_{1/2}$ $\approx$825 ms) and is presumably associated with reduced ferredoxin, as it is not observed in the control sample. It could be ascribed to a recombination reaction between $P700^+$ and reduced ferredoxin. However, this interpretation is probably too simple and some electron escape from reduced ferredoxin to exogenous acceptors is also likely to be involved. This can be inferred from the observation that the amplitude corresponding to the slowest decay phase ($t_{1/2}$ $\approx$6 s) is considerably larger in the cross-linked sample than in the control. Such an electron escape from fully reduced flavodoxin was essentially absent in the PSI–flavodoxin covalent complex

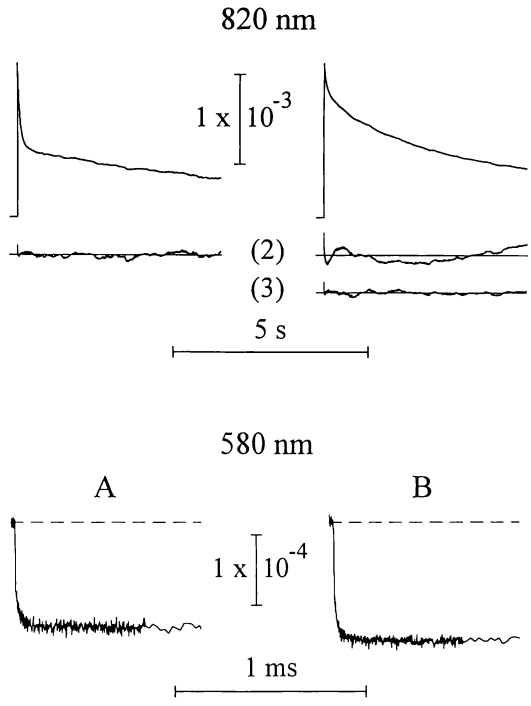

Fig. 1. Flash-induced absorption changes of PSI complexes (control) and PSI complexes cross-linked with ferredoxin (PSI–ferredoxin) at 580 and 820 nm. Experimental conditions: 20 mM tricine pH 8.0, 2 mM sodium ascorbate, 25 μM DPIP (580 nm) or 1.5 μM DPIP (820 nm), 0.03% β-DM, 0.26 μM PSI or PSI–ferredoxin, both from *Synechocystis* sp. PCC 6803. Band width DC-1 MHz (580 nm) or DC-30 kHz (820 nm). Repetition rate: 1 flash every 60 s (820 nm) or 10 s (580 nm). Average of 16 (820 nm) or 64 experiments (580 nm). Upper part: left, control; right, PSI–ferredoxin. Traces (2) and (3): corresponding residuals of fits with either two or three exponential components (multiplied by 3). Results of the fits: left trace 2, two components: $t_{1/2}$ = 46 ms (0.92×10^{-3}) and 6.2 s (0.76×10^{-3}); right trace 2, two components: $t_{1/2}$ = 122 ms (0.38×10^{-3}) and 4.0 s (1.25×10^{-3}); right trace 3, three components: $t_{1/2}$ = 44 ms (0.27×10^{-3}), 825 ms (0.44×10^{-3}) and 6.5 s (0.96×10^{-3}). Lower part: traces A and B correspond to the differences between flash-induced absorption changes recorded at 580 nm in the cross-linked and control samples, at pH 8.0 and 5.8 respectively. These traces put forward directly the process of ferredoxin reduction in the cross-linked sample.

(Mühlenhoff *et al.*, 1996) and probably reflects the different reactivities of the two proteins towards exogenous acceptors. The amount of ferredoxin reduction in the cross-linked complex nevertheless can be estimated from the comparison of the fastest phase amplitudes, which represent 55 and 16% of the total decay in the control and cross-linked samples respectively. The corresponding 70% decrease in amplitude in the cross-linked sample versus the control can be interpreted by assuming that the laser flash triggers the reduction of 0.7 ferredoxin per PSI in the cross-linked sample. In brief, experiments at 820 nm indicate that the recombination reaction between $P700^+$ and $(F_A, F_B)^-$ is 70% inhibited in the cross-linked complex compared with the control sample. This indicates that ferredoxin is most probably reduced by $(F_A, F_B)^-$ in 70% of the PSI reaction centers.

As previously shown (Sétif and Bottin, 1994, 1995), the reduction of ferredoxin by PSI can be monitored directly in the 460–600 nm region. This was performed

in the present study by comparing the absorption changes in the control and cross-linked samples after precisely adjusting their concentrations. This adjustment was done at the red maximum of chlorophyll absorption. The margin of error is <0.2% so that the absorption transients recorded on the two samples can be compared directly. The difference between traces recorded at pH 8.0 in the cross-linked sample and in the control is shown at 580 nm in the lower part of Figure 1 (curve A). Such a procedure is used in order to put forward directly the kinetics of ferredoxin reduction while subtracting some antenna signals (Sétif and Bottin, 1994, 1995). A very fast phase (submicrosecond component) is present in these kinetics, which is unresolved with the time resolution of the setup. This decay is followed at 580 nm by a prominent phase of $t_{1/2} \approx 13$ μs. It can be noted that the same signal of ferredoxin reduction is observed either in the absence of salts (data shown in Figure 1) or in the presence of 30 mM NaCl and 5 mM $MgCl_2$. Flash absorption transients were also recorded at pH 5.8 (no salts). Under these conditions, the difference between the signals observed at 580 nm in the two samples is also shown in Figure 1 (lower part, curve B). The kinetics are biphasic, similar to those observed at pH 8.0, but exhibit slightly different features: the amplitude of the submicrosecond phase is larger, as is the total amplitude; the second phase is slightly faster ($t_{1/2} \approx 10.5$ μs).

Traces similar to those recorded at 580 nm were obtained from 460 to 600 nm for the control and the cross-linked samples, and the corresponding differences were calculated by the same procedure as described above. A global fit procedure was used for fitting the data recorded in the whole spectral range. For the kinetics recorded at pH 8, the data were only poorly fitted by assuming only one microsecond component. However, the data could be very well fitted with two microsecond components, resulting in half-times of 13.5 and 380 μs. A faster submicrosecond component was present at any wavelength above 460 nm and was taken as the initial amplitude after the flash which results from the fitting procedure. The spectral shape of the three components ($t_{1/2}$ <1, ≈13.5 and 380 μs) of ferredoxin reduction observed in the cross-linked complex are rather similar to the spectra of the three components observed at pH 8 in the presence of salts with free ferredoxin ($t_{1/2}$ <1, ≈13–20 and 103–120 μs; Sétif and Bottin, 1995). For example, the largest spectral amplitude is found at 480–500 nm for the 380 μs component. To obtain an estimate of the contributions of the three different phases in the reduction of ferredoxin, their spectra were integrated between 460 and 600 nm. This procedure gives amounts of 46, 39 and 15% for the contributions of the submicrosecond phase, the intermediate phase (13.5 μs) and the slowest phase (380 μs), respectively. The slowest component therefore appears minor, contrary to what is observed with free ferredoxin where its represents one third of the total amplitude of ferredoxin reduction (Sétif and Bottin, 1995). When the above global fit procedure was used to fit the data observed at pH 5.8, a single microsecond component was found with a $t_{1/2} \approx 10.5$ μs. As is found at pH 8, a submicrosecond phase was also found at any wavelength above 460 nm. By using the same integration procedure as above, contributions of 56 and 44% were found for the submicrosecond phase and the 10 μs phase respectively.

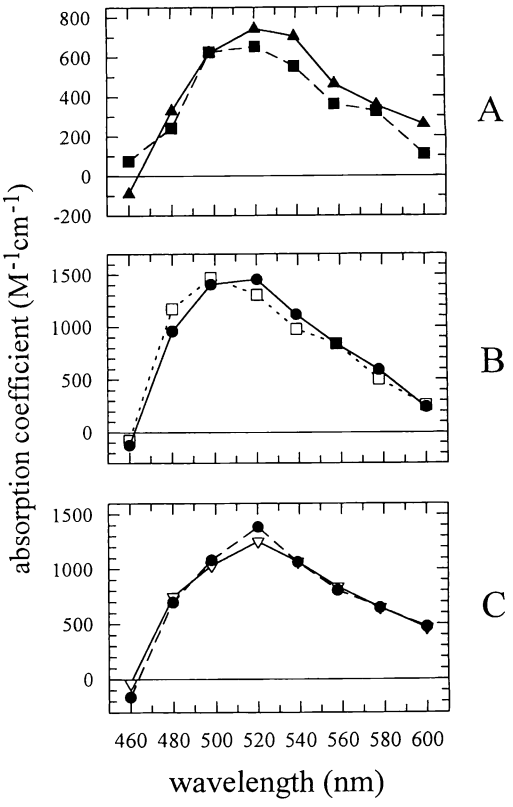

Fig. 2. Decay-associated spectra due to ferredoxin reduction in the covalent PSI–ferredoxin complex. Each spectrum results from a global fit analysis of a series of absorption changes obtained between 460 and 600 nm. Each of these changes corresponds to a difference between flash-induced absorption changes recorded in the covalent complex and in a control sample, under conditions similar to those of Figure 1. The vertical scales are given by reference to the signal of $P700^+$ at 820 nm (assuming $\varepsilon = 6500\ M^{-1}\ cm^{-1}$). (**A**) Amplitude of the submicrosecond component at pH 5.8 (closed triangles) or pH 8.0 (closed squares). (**B**) Sum of the amplitudes of the three components observed at pH 8.0 (closed circles); the calculated spectrum corresponding to electron transfer from $(F_A, F_B)^-$ to ferredoxin is also shown (open squares) after multiplication by a scaling factor of 0.57. (**C**) Sum of the amplitudes of the two components observed at pH 5.8 (closed circles); the spectrum recorded under similar conditions with free ferredoxin is also shown (open triangles) after multiplication by a scaling factor of 0.60.

The spectra of the submicrosecond components for both pH values are shown in Figure 2A (pH 5.8: triangles; pH 8: squares). Their amplitudes were calculated by reference to the signal of $P700^+$ at 820 nm (assuming $\varepsilon = 6500\ M^{-1}\ cm^{-1}$). An absorption decrease is shown here as positive as it corresponds to a positive amplitude in a decay-associated spectrum. The spectra at both pH values are quite similar and their shapes are fully consistent with the spectrum which can be calculated independently for the reduction of ferredoxin by (F_A, F_B) (open squares in Figure 2B; see Materials and methods). Figure 2B shows the spectrum corresponding to the three phases observed at pH 8 (closed circles) together with the calculated spectrum. For spectral comparison, this calculated spectrum was multipled by a factor of 0.57. This scaling factor is chosen so that similar values are found for the two spectra when integrated between 460 and 600 nm. The observed and calculated spectral shapes match very closely, which shows unambiguously that the

observed kinetics correspond to ferredoxin reduction. The spectrum corresponding to the sum of the two phases observed at pH 5.8 ($t_{1/2}$ <1 μs and ≈10 μs) is shown in Figure 2C (closed circles). It closely matches the corresponding spectrum observed at the same pH value with free ferredoxin (open triangles; Sétif and Bottin, 1995). This last spectrum (corresponding to almost full ferredoxin reduction) was multiplied by a factor of 0.60 to normalize the integrated spectra. It was found previously that this spectrum deviates somewhat from the calculated spectrum (compare open squares of Figure 2B and open triangles of Figure 2C; Sétif and Bottin, 1995). However, it is interesting to note that the same spectral deviations are observed in the cross-linked complex. Moreover, the spectra obtained for the cross-linked complex indicate similar yields for ferredoxin reduction at both pH values (57–60% of reduced ferredoxin per PSI reaction center). By comparison with signals obtained with free ferredoxin, these flash-induced absorption changes in the visible region thus clearly show fast reduction of ferredoxin in ~60% of the PSI reaction centers. Moreover, the observed rates indicate that ferredoxin is bound to PSI in a position which is very similar to that in the non-covalent complex.

Study of electron transfer between the covalent complex and soluble partners

In order to test how many ferredoxin binding sites are occupied and to check the (in)ability of the PSI–ferredoxin cross-linked complex to reduce soluble ferredoxin or flavodoxin, the kinetics of ferredoxin and flavodoxin reduction by both this complex and isolated PSI, pre-treated with the chemical cross-linking reagents, were measured at 580 nm. The results of such experiments are shown in Figure 3. The upper part displays the effect of ferredoxin addition directly. Whereas the kinetics of ferredoxin reduction do not appear to be affected by the chemical treatments (curve co for the control experiment), a signal of similar kinetics but of a 5-fold decrease in amplitude can be detected for the covalent complex preparation (curve cl). This signal was obtained with a ferredoxin concentration of 2 μM. A higher ferredoxin concentration did not result in a significant increase in signal size, thus indicating that only ~20% of the cross-linked PSI reaction centers are able to reduce free ferredoxin. In the case of flavodoxin (lower part of Figure 3), first-flash experiments exhibiting the formation of the flavodoxin semiquinone (Mühlenhoff and Sétif, 1996) were recorded after addition of 20 μM flavodoxin (from *Synechococcus* 7002) in darkness. The control experiments without flavodoxin (curve 0) are similar whether PSI is pre-treated with the chemical cross-linking reagents, or not. The absorption increase due to flavodoxin reduction is about four times smaller in the cross-linked complex (curve cl) than in the control sample (curve co), indicating that ~25% of the cross-linked centers still show reduction of free flavodoxin; the kinetics of both signals (curves co and cl) are similar ($t_{1/2}$ ≈1.5 ms). These results indicate very similar binding characteristics of both flavodoxin and ferredoxin in our experiments. It also appears very likely that, in 20–25% of the reaction centers, ferredoxin is not bound at the normal binding site. Moreover, in these reaction centers, this 'wrong' binding allows reduction of free ferredoxin or flavodoxin with normal rates.

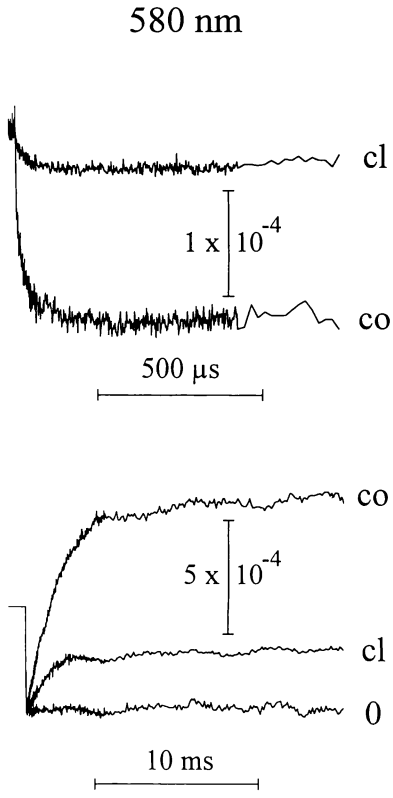

Fig. 3. Upper part: differences between flash-induced absorption changes measured at 580 nm in the presence (2.02 μM) and in the absence of soluble ferredoxin from *Synechocystis* 6803. Experimental conditions: 0.26 μM PSI, in 20 mM tricine pH 8.0, 0.03% β-DM, 2 mM sodium ascorbate, 15 μM DPIP, 5 mM $MgCl_2$ and 30 mM NaCl; curve cl, PSI–ferredoxin covalent complex; curve co, isolated PSI, treated with EDC in the absence of ferredoxin. Each trace corresponds to the difference between averaged signals (32 flashes) recorded in the presence and absence of ferredoxin. Lower part: flash-induced absorption changes measured at 580 nm in the absence (curve 0) or in the presence (curves cl and co) of 20 μM of flavodoxin from *Synechococcus* 7002. Experimental conditions were identical to those for the upper part; curve cl, PSI–ferredoxin covalent complex; curve co, isolated PSI, treated with EDC in the absence of ferredoxin. Curve 0 corresponds to an average of eight experiments. Curves cl and co are first-flash experiments recorded after addition of flavodoxin in darkness. The signals from three different samples were averaged in both cases.

EPR characterization of the covalent PSI–ferredoxin complex

Spin quantitation was performed at 30 K under non-saturating conditions for estimating the ferredoxin content of the covalent complex, as previously described (Lelong *et al.*, 1994). This was done on the same preparation that was used for flash absorption spectroscopy. The spin content was compared under highly reducing conditions (F_A and F_B reduced; little F_X reduced; ferredoxin reduced when present) between a cross-linked sample and a control sample. These experiments indicate the presence of 1.17 ± 0.08 ferredoxin per PSI reaction center in the covalent complex. Though this indicates that the covalent complex contains slightly more ferredoxin than PSI, the above number is in accordance, within the given uncertainties, with previous measurements (Lelong *et al.*, 1994).

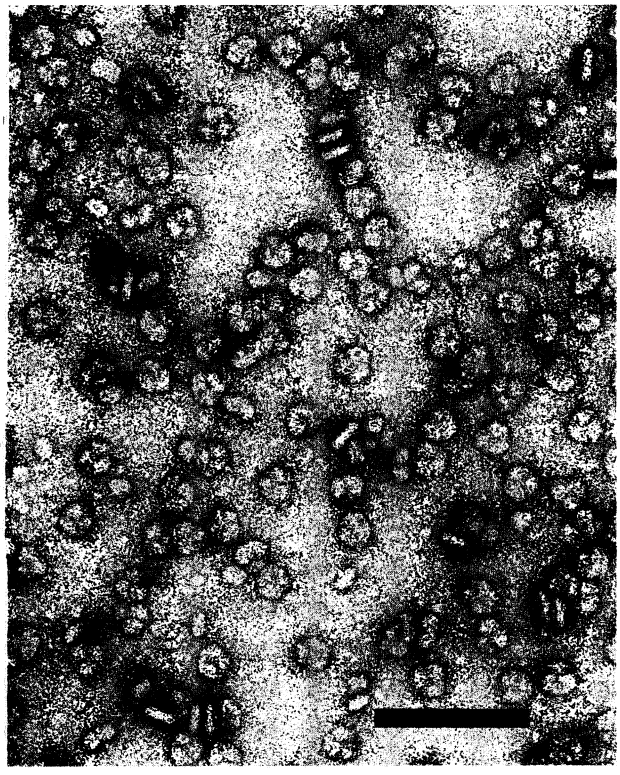

Fig. 4. Electron microscopy of trimeric PSI from *Synechocystis* 6803 cross-linked to ferredoxin. Part of an electron micrograph showing PSI–ferredoxin particles in top and side view positions. Particles were negatively stained with uranyl acetate. Scale bar represents 1000 Å.

Analysis of projections obtained by electron microscopy

As an alternative for two-dimensional crystals, trimeric PSI particles can be used for image analysis of electron micrographs at moderate resolution (Boekema *et al.*, 1994). Therefore, cross-linking experiments between PSI and ferredoxin were performed with preparations of trimeric reaction centers. Electron micrographs, such as the one shown in Figure 4, show the characteristic views of trimeric PSI particles cross-linked to ferredoxin. To visualize these views with enhanced resolution, single particle analysis was carried out. From 16 digitized micrographs, 2041 top view projections and 20 side view projections were selected and used for further processing. The top view projections were aligned, treated with multivariate statistical analysis and classified. In previously analyzed data sets of trimeric PSI particles, either two types of projections differing in handedness were found (Boekema *et al.*, 1989; Kruip *et al.*, 1993), or just one type of handedness predominated (Kruip *et al.*, 1993). The classification of the PSI particles cross-linked to ferredoxin showed that there was one type of handedness strongly predominating. When the data set was decomposed into 12 classes (Figure 5), only one class contained some projections with opposing handedness. The largest observed variations reflect differences caused by slight tilting of molecules on the carbon support film. Due to tilting, one of the monomers in the trimer may look substantially smaller than the other two (see e.g. Figure 5B and G). Tilting may also change smaller details, such as the small connecting masses in the center of the trimer, which can be seen rather clearly in the untilted trimers shown in Figure 5I–L. These connecting masses are almost absent in the average projection of most other classes, due to overlap. Thus, in the final summation, the best 225 projections from only four classes I–L, which displayed sharpest detail and pure 3-fold symmetry, were averaged (Figure 6A).

To investigate the height of the PSI–ferredoxin particles, projections were analyzed from pairs of particles that, in side view position, are in close contact with their cytoplasmic sides by artificial aggregation. The projections were aligned repeatedly on improved references, and a final sum was made (Figure 6G). In this final sum, the gap between the two trimeric particles, corresponding to the extrinsic cytoplasm-exposed subunits and ferredoxin, is ~40 Å in width, similar to the gap caused by PsaC, PsaD and PsaE alone (Kruip *et al.*, 1993).

In order to localize the binding site of ferredoxin on PSI, we compared top views of particles cross-linked to ferredoxin (Figure 6A) with two independent data sets of untreated PSI particles (Figure 6B and C). The two data sets gave averaged projections with identical image features up to 20 Å resolution (not shown). Subtraction of the data shown in Figure 6B from those of Figure 6A yields the contoured difference image (Figure 6D) which shows one clear difference area and two areas of weaker intensity. The areas with weaker intensity fall in projection within an area occupied by the peripheral subunits PsaC, PsaD and PsaE which form a ridge on the cytoplasm-exposed side of PSI (Figure 6H). Because they coincide with the ridge, these two areas are interpreted as noise-related for reasons derived from the side view analysis (Figure 6G). If ferredoxin were on top of the ridge, side views would indicate a corresponding increase in thickness in comparison with untreated PSI, which was not observed. In contrast, in treated as well as in untreated PSI, the gap between two PSI particles is ~40 Å, whereas for the cross-linked product of PSI and flavodoxin, it is ~50 Å (Mühlenhoff *et al.*, 1996). Thus, only the area with the highest intensity in Figure 6D should indicate the ferredoxin position.

The fact that the difference is not very intense led us to compare various average images more closely. First, the set of the best 591 projections of the cross-linked complex (classes I–L of Figure 5) was divided randomly into two halves by taking either odd or even numbered projections. From each half-set, the best 225 projections were summed. The difference image between the two 225 projection sums shows the highest minima and largest maxima to be four times smaller than the highest peak in the difference map of cross-linked and native data. This is outlined by only one contour level in Figure 6E. Second, a difference map between the two average sums of native complex (Figure 6F) was produced by subtraction of images of Figure 6B and C. It should be noted that these last images were the results of strictly separated analyses of micrographs originating from different protein batches. Nevertheless, the highest minimal and largest maximal densities in the difference image of Figure 6F are outlined by only two contour levels. These intensities are twice as small as the highest peak in the difference map between cross-linked and native data, which is outlined by four levels (Figure 6D). From this, we conclude that the highest peak in the latter difference map is unambiguously

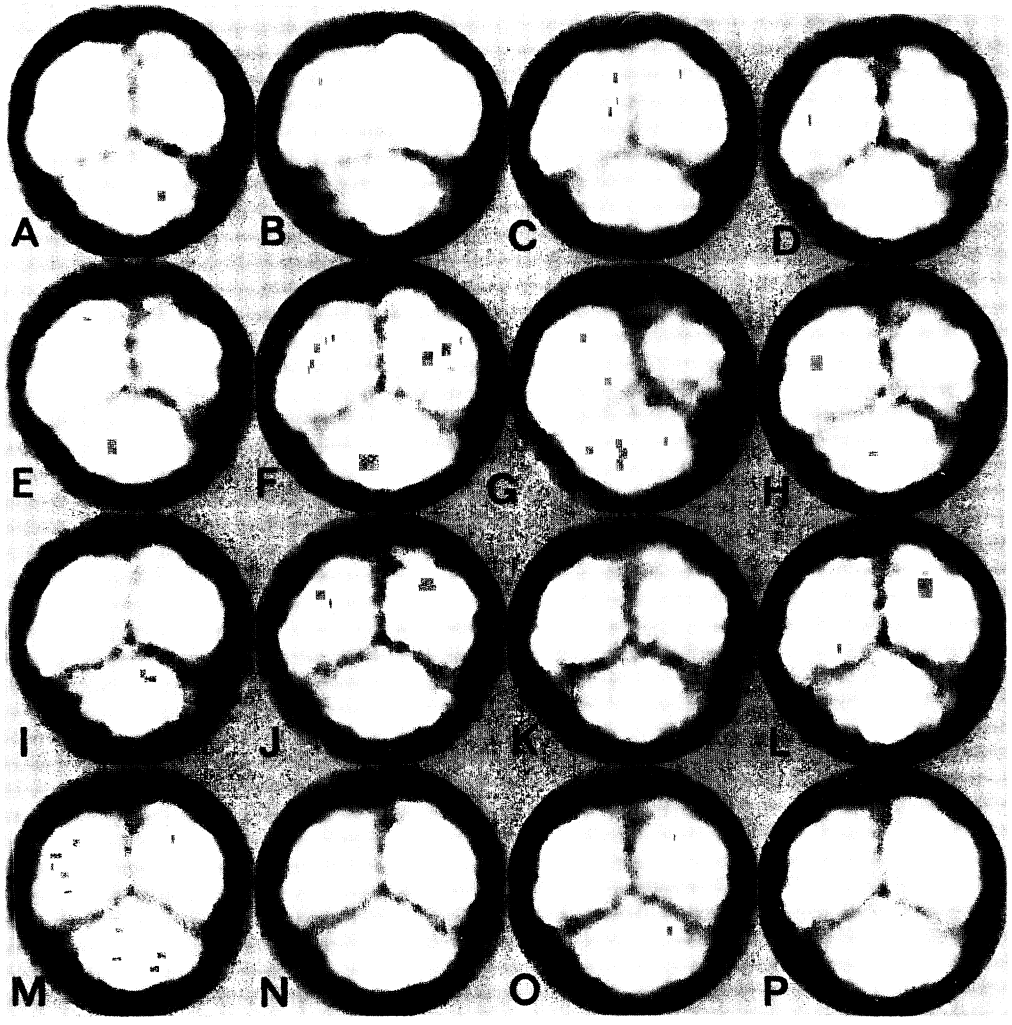

Fig. 5. Classification of 2041 top view projections, which were aligned and treated with multivariate statistical analysis. The data set was decomposed into 12 classes with 119 (**A**), 156 (**B**), 92 (**C**), 125 (**D**), 154 (**E**), 156 (**F**), 181 (**G**), 131 (**H**), 167 (**I**), 139 (**J**), 158 (**K**) and 157 (**L**) members, respectively. The four classes (I–L) showing the best preserved 3-fold rotational symmetry are also presented with this symmetry imposed (**M–P**). During classification 15% of the data set was automatically rejected.

correlated with the localization of ferredoxin in the cross-linked complex.

Discussion

Several characteristics of the PSI–ferredoxin complex which is studied here were determined previously (Lelong *et al.*, 1994): the amino acid of each polypeptide involved in the covalent bond (ferredoxin and subunit PsaD of PSI) was identified and the presence of one ferredoxin per PSI reaction center, which could be reduced after continuous illumination, was observed by EPR. The present results extend this first characterization much further, towards an understanding of the structural and functional interaction of PSI with ferredoxin.

In the cross-linked PSI–ferredoxin complex, the ferredoxin reduction process is very similar to that observed in the normal complex with free ferredoxin: two and three phases are present at pH 5.8 and 8.0 respectively. The corresponding phases observed with the normal complex were identified previously with first order processes and were ascribed to electron transfer within PSI–ferredoxin complexes which are preformed before flash excitation (Sétif and Bottin, 1994, 1995). The rates and the spectra of these phases are very similar in both types of complex, with the exception of the slowest phase observed at pH 8. In the covalent complex, this phase is about three times slower and its amplitude is about twice as small as in the normal complex. A prominent submicrosecond phase of ferredoxin reduction (~50% of the total amplitude after one flash) is present at both pH values. However, the total signal amplitude corresponding to ferredoxin reduction represents only ~60% of the amplitude which is expected for one ferredoxin reduced per reaction center. A percentage of 70% of ferredoxin reduction can be also calculated from the analysis of $P700^+$ decay.

These data clearly indicate that ferredoxin has been cross-linked correctly to its physiological binding site in 60–70% of the reaction centers. It should be emphasized that the existence of a submicrosecond phase of ferredoxin reduction in the covalent complex probably means that the ferredoxin locations in the covalent and normal complexes are identical. In 20–25% of the reaction centers, $(F_A, F_B)^-$ is still able to reduce soluble acceptors. This result, together with the spin quantitation results, suggests that in these centers ferredoxin is possibly bound in a

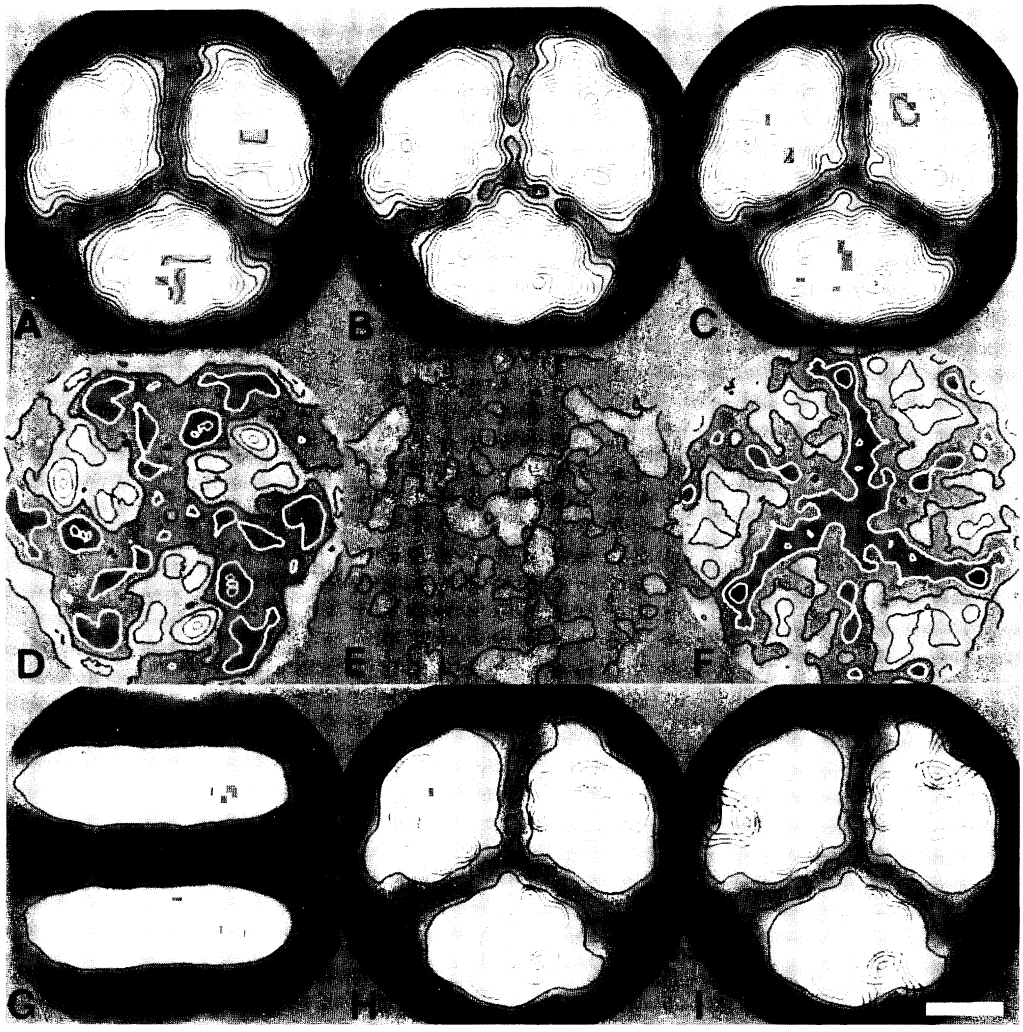

Fig. 6. Comparison of final results of single particle averaging of trimeric *Synechocystis* 6803 PSI projections. (**A**) Sum of the best 225 top view projections (from classes I–L of Figure 5) of a PSI–ferredoxin covalent complex. (**B**) Sum of the best 150 top view projections (out of 1464) of control PSI. (**C**) Sum of the best 114 top view projections (out of 898) of a second independent control PSI (modified from Kruip *et al.*, 1993). (**D**) The difference image between the normalized images of (A) and (B). (**E**) The difference image between two sums of 225 images, randomly taken from the best 450 images of classes I–L from Figure 5. (**F**) The difference image between two sets of normalized images of (B) and (C). (**G**) Sum of 20 side view projections of PSI particles cross-linked to ferredoxin, aggregated with their stromal-exposed sides. (**H**) Image of (A) on which the lowest two contours of image (B) have been superimposed, as well as the highest three levels of image (D) and contour levels of a difference image from the peripheral subunits PsaC, PsaD and PsaE (determined in Kruip *et al.*, 1993 and by J.Kruip, M.Rögner and E.J.Boekema, unpublished data). (**I**) Image as shown in (H), on which additionally a flavodoxin difference image in the contours-only version has been superimposed (from Mühlenhoff *et al.*, 1996). Contours are all on the same scale; positive density is marked by black contours, negative density [only indicated in (D) and (F)] is marked by white contours. Scale bar represents 50 Å.

position which is not compatible with fast reduction and which does not impede docking of free soluble acceptors at their normal binding site.

Our location of ferredoxin, with its mass center 77 Å away from the 3-fold axis of the PSI trimers, gives experimental evidence for a hypothetical site (Fromme *et al.*, 1994) postulated by modeling the ferredoxin atomic structure onto the PSI structure obtained from X-ray analysis of three-dimensional crystals at 6 Å resolution (Krauss *et al.*, 1993). The hypothetical binding site for ferredoxin presented in that study is very similar to the location found in the present investigation. A precise comparison, however, cannot be given owing to the lack of distance parameters in the presentation of the model (Fromme *et al.*, 1994). The upper part of Figure 7 exhibits the contours of both PSI and ferredoxin (taken from Figure 6H), together with the locations of the terminal acceptors F_I and F_{II} as deduced from the X-ray structure of PSI (Krauss *et al.*, 1993). This view emphasizes that, within the cross-linked complex, the [2Fe–2S] center of ferredoxin is closer to the [4Fe–4S] center F_{II} of PSI than to F_I. The consequences of this observation on the electron transfer kinetics within the cross-linked complex are outlined in greater detail in the lower part of Figure 7. As the electron transfer rate is strongly distance dependent (Marcus and Sutin, 1985; Moser *et al.*, 1992), it is very likely that ferredoxin cannot be reduced directly by center F_I but rather is reduced by center F_{II}. When considering the presence of a submicrosecond phase of ferredoxin reduction in the covalent complex, this has an important implication regarding the electron transfer rates within PSI, i.e. F_{II} is probably reduced in <1 μs. This result is at variance with recent photovoltage measurements with a microsecond time resolution (Sigfridsson *et al.*, 1995),

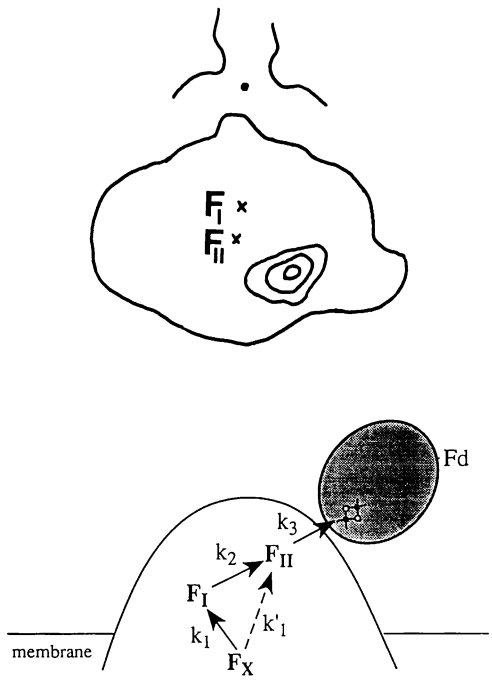

Fig. 7. Upper part: schematic top view of the PSI–ferredoxin covalent complex (from Figure 6H) showing the contours which are attributed to ferredoxin together with the positions of the terminal iron–sulfur centers of PSI. Lower part: schematic view of the interactions between PSI and ferredoxin, emphasizing that F_{II} is most probably the partner of the [2Fe–2S] center of ferredoxin during electron transfer. The rates of electron transfer, which are compatible with the present study together with that of Leibl *et al.* (1995), are also indicated.

from which it was proposed that F_{II} (identified by the authors with F_A) is reduced with a lifetime of 30 µs. Another study with a higher time resolution shows that (F_A, F_B) is most probably reduced with a half-time of <50 ns, the reduction of F_X ($t_{1/2}$ ≈150–200 ns) being the rate-limiting step of forward electron transfer within PSI (Leibl *et al.*, 1995). However, this study did not yield information on any microsecond electrogenic component which could be due to electron transfer from F_I to F_{II}. The lower part of Figure 7 shows the electron transfer rates within PSI which are compatible with the present study and with the photovoltage measurements of Leibl *et al.* (1995).

The ferredoxin binding position can be compared with the binding position of flavodoxin (Figure 6I), as previously determined (Mülhenhoff *et al.*, 1996). Both binding positions partly overlap in an area next to the ridge formed by subunits PsaC, PsaD and PsaE. Is is interesting, however, that both projected densities are not concentric towards each other. Flavodoxin, with its larger size, extends more to the periphery, which must be a consequence of the geometry of the ridge and of the structure of ferredoxin and flavodoxin. X-ray structures show that the [2Fe–2S] cluster in ferredoxin (Tsukihara *et al.*, 1981, 1990; Rypniewski *et al.*, 1991; Ikemizu *et al.*, 1994) and the FMN group in flavodoxin (Laudenbach *et al.*, 1987; Fukuyama *et al.*, 1992; Rao *et al.*, 1992) are both located towards the outer end of the molecule. This could indicate that both proteins firstly share a common PSI binding site and secondly try to arrange their prosthetic group as close as possible to the terminal PSI electron acceptors in PSI, the iron–sulfur centers of subunit PsaC (and especially F_{II}) being located in the middle of the ridge. Functionally, this should facilitate more rapid electron transfer between the iron–sulfur centers of PsaC and the electron acceptor proteins. This in turn is consistent with a slightly more peripheral location of larger flavodoxin relative to ferredoxin as shown in this study.

Materials and methods

Biological materials and chemical cross-linking

Ferredoxin from *Synechocystis* 6803 was isolated and purified according to Bottin and Lagoutte (1992). PSI from *Synechocystis* 6803 was isolated as described by Rögner *et al.* (1990) and Kruip *et al.* (1993). The trimeric status of the preparation was confirmed by HPLC–gel filtration. Chemical cross-linking between PSI trimers and ferredoxin from *Synechocystis* 6803 was performed as described by Lelong *et al.* (1994). PSI trimers (0.2 mg chlorophyll/ml) were incubated either in the presence or absence (control PSI sample) of 10 µM ferredoxin with 2 mM *N*-ethyl-3-(3-dimethylaminopropyl)carbodiimide (EDC), 2 mM sulfo-*N*-hydroxysulfosuccinimide (NHS) in 20 mM HEPES–NaOH pH 7.5, 5 mM $MgCl_2$ and 0.03% *n*-dodecyl β-D-maltoside (β-DM) for 30 min at room temperature. The reaction was stopped by the addition of 0.5 M ammonium acetate to a final concentration of 0.1 M. The PSI–ferredoxin covalent complex was then washed with 20 mM tricine–NaOH, pH 7.8 containing 0.03% β-DM by ultrafiltration with a Centriprep 100 filter (Amicon) to eliminate chemical reagents and free ferredoxin and to concentrate PSI. The washing procedure was repeated several times.

Flash absorption spectroscopy

Measurements were made at 296 K with a microsecond time resolution as described previously (Sétif and Bottin, 1994, 1995). For identifying absorption signals due to reduction of ferredoxin in the cross-linked complex, a control cuvette containing PSI which had been pre-treated with EDC in the absence of ferredoxin was studied. The absorption spectra of the two cuvettes (control and cross-linked samples) were adjusted at the red maximum of chlorophyll (OD ≈1.5 at 679 nm). The spectra of the two samples were found to be identical in the whole visible region (ΔOD <0.002) and the P700 concentrations of the two samples, calculated from the initial amplitudes of the flash absorption signals at 820 nm, were found to be identical within <0.5%. This indicates that the antenna content of both samples is identical, thus allowing the absorption changes due to ferredoxin to be extracted reliably. The difference spectrum corresponding to the one-electron reduction of (F_A, F_B) was measured by flash absorption spectroscopy in PSI from *Synechocystis* 6803 as described previously (Sétif and Bottin, 1995). The PSI concentration of the samples was calculated from the photoinduced absorption changes at 820 nm assuming an absorption coefficient of 6500/M/cm for $P700^+$ at this wavelength (Mathis and Sétif, 1981). Data were fitted with several exponential components using a Marquardt algorithm. A global fit procedure was used (Beechem, 1992) for obtaining spectra in the 460–600 nm region.

Electron microscopy and image analysis

For electron microscopy, a drop (4 µl) of a PSI preparation (diluted with 5 mM MES buffer, pH 6.5 plus 0.03% β-DM to 10 µg chlorophyll/ml) was prepared on carbon-coated grids, which were blotted off after 2 min. The grids were washed once with distilled water for a few seconds to reduce the background, and negative stained with 2% uranyl acetate. Electron microscopy was performed with a Jeol JEM 1200 EX electron microscope with 80 kV at ~60 000× magnification. Electron micrographs were digitized with a Kodak Eikonix Model 1412 CCD camera using a scan step size of 25 µm. Image analysis was carried out on a Silicon Graphics Indy workstation using IMAGIC software. In the first step after particle selection, selected images were band-pass filtered to remove the very fine and very coarse image features (Harauz *et al.*, 1988). In the next step the images were aligned with correlation techniques, starting with one noisy single projection as a first reference. Subsequent

references were constructed from the sums of the best aligned particles from a previous alignment (Boekema and Böttcher, 1991). In the following step, the aligned non-symmetrized particles were submitted to multivariate statistical analysis and automatic classification (Harauz *et al.*, 1988). Next, the members of each class were summed, but in a slightly different way from that described earlier (Kruip *et al.*, 1993): for the final sums, the images to be summed were shifted rotationally and translationally using the parameters that were calculated when they were aligned with the band-pass filter imposed. In the last step, final sums were 3-fold rotationally symmetrized.

Acknowledgements

We would like to thank Dr U.Mühlenhoff for providing us with flavodoxin from *Synechococcus* sp. PCC 7002, Dr W.Keegstra for his help with computer image analysis and Dr P.Fromme for her help in drawing Figure 7. The work of E.J.B. is supported by EC grant BIOT 2CT 930087. M.R. is grateful for support from the Deutsche Forschungsgemeinschaft (DFG) and from the Research Institute of Innovative Technology for the Earth (RITE, Japan).

References

Aliverti,A., Corrado,M.E. and Zanetti,G. (1994) *FEBS Lett.*, **343**, 247–250.

Andersen,B., Koch,B. and Scheller,H.V. (1992) *Physiol. Plant.*, **84**, 154–161.

Batie,C.J. and Kamin,H. (1984a) *J. Biol. Chem.*, **259**, 8832–8839.

Batie,C.J. and Kamin,H. (1984b) *J. Biol. Chem.*, **259**, 11976–11985.

Beechem,J.M. (1992) *Methods Enzymol.*, **210**, 37–54.

Bhattacharyya,A.K., Meyer,T.E. and Tollin,G. (1986) *Biochemistry*, **25**, 4655–4661.

Boekema,E.J. and Böttcher,B. (1991) *Biochim. Biophys. Acta*, **1098**, 131–143.

Boekema,E.J., Dekker,J.P., Rögner,M., van Heel,M.G. and Witt,H.T. (1989) *Biochim. Biophys. Acta*, **974**, 81–87.

Boekema,E.J., Boonstra,A.F., Dekker,J.P. and Rögner,M. (1994) *J. Bioenerg. Biomembr.*, **26**, 17–29.

Bottin,H. and Lagoutte,B. (1992) *Biochim. Biophys. Acta*, **1101**, 48–56.

Correll,C.C., Batie,C.J., Ballou,D.P. and Ludwig,M. (1992) *Science*, **258**, 1604–1610.

De Pascalis,A.R., Jelesarov,I., Ackermann,F., Koppenol,W.H., Hirasawa,M., Knaff,D.B. and Bosshard,H.R. (1993) *Protein Sci.*, **2**, 1126–1135.

De Pascalis,A.R., Schürmann,P. and Bosshard,H.R. (1994) *FEBS Lett.*, **337**, 217–220.

Fromme,P., Schubert,W.-D. and Krauss,N. (1994) *Biochim. Biophys. Acta*, **1187**, 99–105.

Fukuyama,K., Matsubara,H. and Rogers,L.J. (1992) *J. Mol. Biol.*, **225**, 775–789.

Golbeck,J.H. (1993) *Curr. Opin. Struct. Biol.*, **3**, 508–514.

Harauz,G., Boekema,E.J. and Van Heel,M. (1988) *Methods Enzymol.*, **164**, 35–49.

Hirasawa,M., Boyer,J.M., Gray,K.A., Davis,D.J. and Knaff,D.B. (1987) *FEBS Lett.*, **221**, 343–348.

Hirasawa,M., Chang,K.-T. and Knaff,D.B. (1991) *Arch. Biochem. Biophys.*, **286**, 171–177.

Hirasawa,M., Tollin,G., Salamon,Z. and Knaff,D.B. (1994a) *Biochim. Biophys. Acta*, **1185**, 336–345.

Hirasawa,M., Proske,P.A. and Knaff,D.B. (1994b) *Biochim. Biophys. Acta*, **1187**, 80–88.

Hurley,J.K. *et al.* (1993a) *Biochemistry*, **32**, 9346–9354.

Hurley,J.K., Cheng,H., Xia,B., Markley,J.L., Medina,M., Gomez-Moreno,C. and Tollin,G. (1993b) *J. Am. Chem. Soc.*, **115**, 11698–11701.

Hurley,J.K., Medina,M., Gomez-Moreno,C. and Tollin,G. (1994) *Arch. Biochem. Biophys.*, **312**, 480–486.

Ikemizu,S., Bando,M., Sato,T., Morimoto,Y. and Tsukihara,T. (1994) *Acta Crystallogr.*, **D50**, 167–174.

Jelesarov,I., De Pascalis,A.R., Koppenol,W.H., Hirasawa,M., Knaff,D.B. and Bosshard,H.R. (1993) *Eur. J. Biochem.*, **216**, 57–66.

Karplus,P.A. and Bruns,C.M. (1994) *J. Bioenerg. Biomembr.*, **26**, 89–99.

Knaff,D.B. and Hirasawa,M. (1991) *Biochim. Biophys. Acta*, **1056**, 93–125.

Krauss,N. *et al.* (1993) *Nature*, **361**, 326–330.

Kruip,J., Boekema,E.J., Bald,D., Boonstra,A.F. and Rögner,M. (1993) *J. Biol. Chem.*, **268**, 23353–23360.

Kruip,J., Bald,D., Hankamer,B., Nield,J., Boonstra,A.F., Barber,J., Boekema,E.J. and Rögner,M. (1995) In Mathis,P. (ed.), *Photosynthesis: from Light to Biosphere. Proceedings of the Xth International Congress of Photosynthesis.* Kluwer, Dordrecht, **3**, pp. 405–408.

Laudenbach,D.E., Straus,N.A., Pattridge,K.A. and Ludwig,M.L. (1987) In Edmonson,D.E. and McCormick,D.B. (eds), *Flavins and Flavoproteins.* de Gruyter, Berlin, pp. 249–260.

Leibl,W., Toupance,B. and Breton,J. (1995) *Biochemistry*, **34**, 10237–10244.

Lelong,C., Sétif,P., Lagoutte,B. and Bottin,H. (1994) *J. Biol. Chem.*, **269**, 10034–10039.

Mathis,P. and Sétif,P. (1981) *Isr. J. Chem.*, **21**, 316–320.

Marcus,R.A. and Sutin,N. (1985) *Biochim. Biophys. Acta*, **811**, 265–322.

Medina,M., Mendez,E. and Gomez-Moreno,C. (1992) *Arch. Biochem. Biophys.*, **299**, 281–286.

Moser,C.C., Keske,J.M., Warncke,K., Farid,R.S. and Dutton,P.L. (1992) *Nature*, **355**, 796–802.

Mühlenhoff,U. and Sétif,P. (1996) *Biochemistry*, **35**, 1367–1374.

Mühlenhoff,U., Kruip,J., Bryant,D.A., Rögner,M., Sétif,P. and Boekema,E.J. (1996) *EMBO J.*, **15**, 488–497.

Rao,S.T., Shaffie,F., Yu,C., Satyshur,K.A., Stockman,B.J., Markley,J.L. and Sundaralingam,M. (1992) *Protein Sci.*, **1**, 1413–1427.

Rögner,M., Dixon,P.J. and Diner,B.A. (1990) *J. Biol. Chem.*, **265**, 6189–6196.

Rousseau,F., Sétif,P. and Lagoutte,B. (1993) *EMBO J.*, **12**, 1755–1765.

Rypniewski,W.R., Breiter,D.R., Benning,M.M., Wesenberg,G., Oh,B.-H., Markley,J.L., Rayment,I. and Holden,H.M. (1991) *Biochemistry*, **30**, 4126–4131.

Sétif,P. and Bottin,H. (1994) *Biochemistry*, **33**, 8495–8504.

Sétif,P. and Bottin,H. (1995) *Biochemistry*, **34**, 9059–9070.

Sigfridsson,K., Hansson,Ö. and Brzezinski,P. (1995) *Proc. Natl Acad. Sci. USA*, **92**, 3458–3462.

Sonoike,K., Hatanaka,H. and Satoh,S. (1993) *Biochim. Biophys. Acta*, **1141**, 52–57.

Tsukihara,T., Fukuyama,K., Nakamura,M., Katsube,Y., Tanaka,N., Kakudo,M., Hase,T., Wada,K. and Matsubara,H. (1981) *J. Biochem.*, **90**, 1763–1773.

Tsukihara,T., Fukuyama,K., Mizushima,M., Harioka,T., Kusunoki,M., Katsube,Y., Hase,T. and Matsubara,H. (1990) *J. Mol. Biol.*, **216**, 399–410.

Walker,M.C., Pueyo,J.J., Navarro,J.A., Gomez-Moreno,C. and Tollin,G. (1991) *Arch. Biochem. Biophys.*, **287**, 351–358.

Zanetti,G. and Merati,G. (1987) *Eur. J. Biochem.*, **169**, 143–146.

Zanetti,G., Morelli,D., Ronchi,S., Negri,A., Aliverti,A. and Curti,B. (1988) *Biochemistry*, **27**, 3753–3759.

Zilber,A.L. and Malkin,R. (1988) *Plant Physiol.*, **88**, 810–814.

Received on December 5, 1995